



**HAL**  
open science

## **PdO@CoSe<sub>2</sub> Composites: An Efficient Electrocatalysts for Water Oxidation in Alkaline Media**

Abdul Hanan, Muhammad Yameen Solangi, Abdul Jaleel Laghari, Aqeel Ahmed Shah, Umair Aftab, Zahoor Ahmed Ibupoto, Muhammad Ishaque Abro, Muhammad Nazim Lakhan, Irfan Ali, Elmuez Dawi, et al.

### ► To cite this version:

Abdul Hanan, Muhammad Yameen Solangi, Abdul Jaleel Laghari, Aqeel Ahmed Shah, Umair Aftab, et al.. PdO@CoSe<sub>2</sub> Composites: An Efficient Electrocatalysts for Water Oxidation in Alkaline Media. RSC Advances, 2023, 13 (1), pp.743-755. 10.1039/d2ra07340d . hal-04222006

**HAL Id: hal-04222006**

**<https://hal.univ-lorraine.fr/hal-04222006v1>**

Submitted on 1 Oct 2023

**HAL** is a multi-disciplinary open access archive for the deposit and dissemination of scientific research documents, whether they are published or not. The documents may come from teaching and research institutions in France or abroad, or from public or private research centers.

L'archive ouverte pluridisciplinaire **HAL**, est destinée au dépôt et à la diffusion de documents scientifiques de niveau recherche, publiés ou non, émanant des établissements d'enseignement et de recherche français ou étrangers, des laboratoires publics ou privés.



Distributed under a Creative Commons Attribution - NonCommercial 4.0 International License

1 **PdO@CoSe<sub>2</sub> Composites: An Efficient Electrocatalysts for Water Oxidation**  
2 **in Alkaline Media**

3  
4 Abdul Hanan<sup>a</sup>, Muhammad Yameen Solangi<sup>b</sup>, Abdul Jaleel Iaghari<sup>b</sup>, Aqeel Ahmed Shah<sup>c</sup>, Umair  
5 Aftab<sup>\*,b</sup>, Zahoor Ahmed Ibupoto,<sup>j</sup> Muhammad Ishaque Abro<sup>b</sup>, Muhammad Nazim Lakhan<sup>a</sup>,  
6 Irfan Ali Soomro<sup>d</sup>, Elmuez A. Dawi<sup>e</sup>, Abd Al Karim Haj Ismail<sup>e</sup>, Elfatih Mustafa<sup>f</sup>, Brigitte  
7 Vigolo<sup>h</sup>, Aneela Tahira<sup>i</sup>, Zafar Hussain Ibupoto<sup>\*,g</sup>

8 <sup>a</sup>Key Laboratory of Superlight Material and Surface Technology, Ministry of Education, College  
9 of Materials Science and Chemical Engineering, Harbin Engineering University, 150001,  
10 Harbin, PR China.

11 <sup>b</sup>Department of Metallurgy and Materials Engineering, Mehran University of Engineering and  
12 Technology, 76080, Jamshoro, Pakistan.

13 <sup>c</sup>NED University of Engineering and Technology, 75270, Karachi, Pakistan.

14 <sup>d</sup>Institute of Computational Chemistry, College of Chemistry, Beijing University of Chemical  
15 Technology, 100029, Beijing, PR China.

16 <sup>e</sup>Nonlinear Dynamics Research Centre (NDRC), Ajman University, P.O. Box 346, United Arab  
17 Emirates.

18 <sup>f</sup>Department of Science and Technology (ITN), Linköping University, Campus Norrköping,  
19 60174 Norrköping, Sweden

20 <sup>g</sup>Dr. M.A Kazi Institute of Chemistry University of Sindh, Jamshoro, 76080, Pakistan

21 <sup>h</sup>Université de Lorraine, CNRS, IJL, F-54000 Nancy, France

22 <sup>i</sup>Institute of Chemistry, Shah Abdul Latif University Khairpur Mirs, Sindh, Pakistan

23 <sup>j</sup>Faculty of Agricultural Engineering and Technology, PMAS-Arid Agriculture University,  
24 Rawalpindi, Pakistan

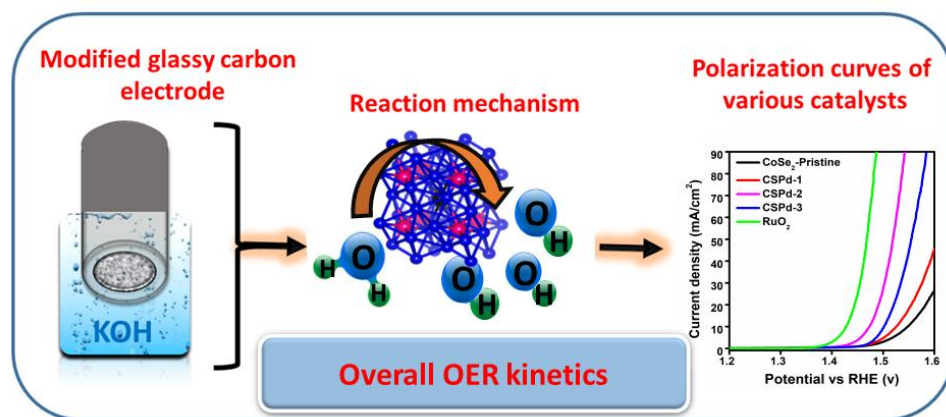
25  
26 **Corresponding author(s):** Zafar Hussain Ibupoto and Umair Aftab

27 **E-mail:** zaffar.ibhupoto@usindh.edu.pk, umair.aftab@faculty.muet.edu.pk

28 **Abstract**

29 In this study, we have prepared cobalt selenide ( $\text{CoSe}_2$ ) due to its useful aspects from catalysis  
30 point of view such as abundant active sites from Se edges, and significant stability in alkaline  
31 conditions.  $\text{CoSe}_2$ , however, has yet to prove its functionality, so we doped palladium oxide  
32 ( $\text{PdO}$ ) onto  $\text{CoSe}_2$  nanostructures using ultraviolet (UV) light, resulting in an efficient and stable  
33 water oxidation composite. The crystal arrays, morphology, and chemical composition of the  
34 surface were studied using a variety of characterization techniques, including X-ray diffraction  
35 (XRD), scanning electron microscopy (SEM), high resolution transmission electron microscopy  
36 (HRTEM), X-ray photoelectron spectroscopy (XPS), and Fourier transform infrared (FTIR). It  
37 was also demonstrated that the composite systems were heterogeneous in their morphology,  
38 undergoing a shift in their diffraction patterns, suffering from a variety of metal oxidation states,  
39 and the surface defects. The water oxidation was verified by a low overpotential of 260 mV at  
40 current density of  $20 \text{ mA/cm}^2$  with Tafel Slope value of  $57 \text{ mVdec}^{-1}$ . The presence of multi metal  
41 oxidation states, rich surface edges of Se and favorable charge transport played a leading role  
42 towards water oxidation at low energy demand. Furthermore, 48 h of durability is associated  
43 with the composite system. With the use of  $\text{PdO}$  and  $\text{CoSe}_2$ , new, low efficiency and simple  
44 electrocatalysts for water catalysis have been developed, enabling the development of practical  
45 energy conversion and storage systems. This is an excellent alternative approach for fostering  
46 growth in the field.

47 **Keywords:**  $\text{PdO@CoSe}_2$  composite, Energy materials, Electrocatalyst, Water Oxidation



**Scheme 1.** Illustration of OER functional surface properties of as-prepared materials

## 48 1. Introduction

49 Fossil fuel use has negatively impacted the environment and led to massive environmental  
50 challenges due to greenhouse gas production<sup>1-3</sup>. Along with the environmental issues caused by  
51 fossil fuel combustion, their reservoirs are rapidly being depleted, posing a strong and acute  
52 threat to life on earth. It is therefore necessary to eliminate greenhouse gases by reducing or  
53 eliminating fossil fuel use, and to produce green fuels with renewable aspects for current and  
54 future uses<sup>4, 5</sup>. Hydrogen energy has been used to build Fuel Cell technology<sup>6, 7</sup>. In the future,  
55 hydrogen and oxygen fuels could be readily obtained for the fulfillment of energy demands  
56 through water splitting<sup>8, 9</sup>. Water splitting can produce hydrogen and oxygen gases using either  
57 photochemical or electrochemical methods. Water splitting requires both water oxidation and  
58 hydrogen evolution reactions (HER) to be driven by efficient catalytic materials. The pre-  
59 requirement for the use of both methods for water splitting is the efficient catalytic material to  
60 drive water oxidation and HER. It is challenging from a kinetics perspective to oxidize water  
61 since four electrons are transferred, and the HER is the simplest process as only two electrons are  
62 transferred<sup>10, 11</sup>. Nevertheless, water oxidation is only limited by the use of precious electro  
63 catalysts such as RuO<sub>2</sub> and IrO<sub>2</sub><sup>12-14</sup>. Rare abundance and high costs limit the use of these noble  
64 materials<sup>15, 16</sup>, indicating that new efficient and cost effective electrocatalyst technology is in  
65 need for water oxidation. Numerous studies have been conducted to find low-cost and earth-  
66 abundant electrocatalysts that foster water oxidation<sup>17, 18</sup>. Various transition-metal based Oxides  
67<sup>19, 20</sup>, Sulfides<sup>21, 22</sup>, Phosphides<sup>23, 24</sup>, Selenides<sup>25</sup> electrocatalysts for water oxidation have been  
68 reported. Extensive studies have been performed for the development of efficient, facile, stable  
69 and earth abundant electrocatalysts for the hydrogen production due the fact that the complete  
70 exploitation of hydrogen fuel from water splitting is restricted by high energy demanding half-  
71 cell water oxidation reaction. As water oxidation is followed by the four-electron transfer  
72 reaction, an effective material is needed to drive significant water oxidation with low energy  
73 requirements.

74 As a result of the availability of multiple metal oxidation states and the unique architecture of  
75 anions as counter anions attached to these multiple metals, researchers have considered the  
76 preparation of bimetallic and polymetallic compounds for electrocatalytic applications, which  
77 have proven more effective than monometallic compounds for water oxidation<sup>26</sup>. In addition,  
78 recent studies indicate that metal oxides and metal selenides perform better as electrocatalysts  
79 than sulfides and phosphides of transition metals<sup>27-30</sup>. Selenides can serve as highly potent

80 catalysts to overcome the above-mentioned challenges for water electrolysis. Se atoms have an  
81 electronic structure of  $4s^24p^4$ , which are easily to gain two electrons from less electronegative  
82 elements to form  $Se^{2-}$  ions, or to share electrons with more electronegative elements to form  
83 TMSes<sup>31</sup>. The TMSes has a high surface area due to its ultrathin layers and the surface  
84 concentration of atoms is also high, which in turn reduces the charge transfer distance thus the  
85 process of water splitting for OER gets accelerated<sup>32</sup>. Due to several reasons, the cobalt selenide  
86 ( $CoSe_2$ ) based electrocatalysts are useful for water oxidation, including their low cost, simple  
87 nature, and significant electrochemical activity<sup>33-36</sup>.

88 Due to its unique synergetic properties and abundant catalytic sites, composite materials are  
89 being made in larger and larger quantities for the development of effective water oxidation  
90 electrocatalysts<sup>37,38</sup>. A wide range of methods have been used to synthesize cobalt-based  
91 nanostructures, including precipitation, vapor deposition, and wet chemical reactions<sup>39-43</sup>.

92 Even though the use of these methods is growing rapidly, there is still a need to adopt facile  
93 approaches for the development of new generation electrocatalysts at a large scale while  
94 incorporating the simple, scalable and tunable features of the nanostructured materials to be  
95 prepared. According to the available literature, PdO nanoparticles have not been doped into  
96  $CoSe_2$  nanostructures via hydrothermal methods followed by UV light reduction. Irradiation of  
97  $PdO@CoSe_2$  by ionizing radiation such as UV-light may break the as-prepared composite bonds  
98 to generate oxygen vacancy defects and therefore increase the OER catalyst's activity due to  
99 increased PdO concentration. Because of the unique three-dimensional electronic configuration  
100 of Co and Pd, as well as the abundance of surface edge sites of Se in the composite systems, the  
101 kinetics of water oxidation are likely to be accelerated with a low energy consumption.

102 The present study investigated the preparation of cobalt selenide ( $CoSe_2$ ) nanostructures by  
103 hydrothermal methods and the doping of palladium oxide (PdO) nanoparticles on them using a  
104 UV irradiation technique to synthesize a composite system represented as  $PdO@CoSe_2$ . Upon  
105 applying 260 mV overpotential to the  $PdO@CoSe_2$  composite, a Tafel slope value of 57 mV/dec  
106 indicated that the effect had a current density of  $20\text{ mA/cm}^2$ .

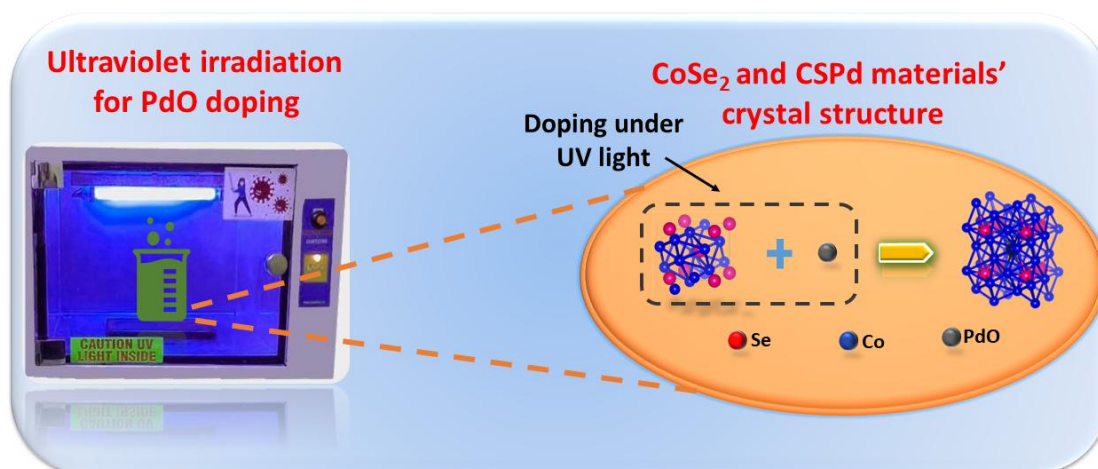
## 107 **2. Experimental work**

### 108 **2.1. Chemical reagents**

109 Cobalt chloride hexahydrate ( $\text{CoCl}_2 \cdot 6\text{H}_2\text{O}$ ), selenium chloride ( $\text{SeCl}_2$ ), palladium chloride  
110 ( $\text{PdCl}_2$ ), hydrazine hydrate ( $\text{N}_2\text{H}_4$ ), hydrochloric acid ( $\text{HCl}$ ) and deionized water were purchased  
111 from Sigma-Aldrich. All the chemicals were of analytical category and used without any further  
112 treatments.

## 113 **2.2. Synthesis of PdO@CoSe<sub>2</sub> composites**

114 Initially, cobalt selenide ( $\text{CoSe}_2$ ) nanostructures were synthesized using hydrothermal  
115 approach that involved dissolving 0.1M cobalt chloride ( $\text{CoCl}_2$ ) in deionized Water (DW) and  
116 stirring for 15 minutes. Then, 0.1M selenium chloride ( $\text{SeCl}_2$ ) was added to above solution at  
117 room temperature under continuous stirring. Later, hydrazine ( $\text{N}_2\text{H}_4$ ) aqueous was added drop  
118 wise into the solution. Then, the mixture was transferred into Teflon-lined stainless-steel  
119 autoclave and put into electric oven instrument using FOTILE 52L at 180°C for 15 hrs. The  
120 hydrothermal autoclave was cooled at room temperature and precipitates of  $\text{CoSe}_2$  were collected  
121 through centrifuge instrument by 4000RPM NSL 80-1. Finally, as-obtained precipitates of  $\text{CoSe}_2$   
122 were washed by DW and dried at 50°C for 5hrs. On the other hand, palladium chloride ( $\text{PdCl}_2$ )  
123 solution was prepared by dissolving 30 mg into 0.02 M HCl. Three different composite samples  
124 were prepared by using 100 mg cobalt selenide ( $\text{CoSe}_2$ ) with varying ratio of palladium (Pd)  
125 solution as 5 mL, 10 mL, and 15 mL into 100 mL of DW and marked as CSPd-1, CSPd-2, CSPd-  
126 3 respectively. Samples were placed in Ultrasonic bath for 20 min. The samples were then placed  
127 in an ultraviolet light chamber with magnetic stirring for 2 hrs to ensure adequate doping of PdO  
128 nanoparticles (PdNPs) on the surface of  $\text{CoSe}_2$ . After the completion of process, samples were  
129 taken from the UV chamber and washed several times with DW before being dried at 60°C under  
130 vacuum conditions. Scheme 2 depicts a schematic representation of PdO nanoparticles doping  
131 onto  $\text{CoSe}_2$  under UV irradiation.



**Scheme 2.** Illustration of overall doping of PdO onto CoSe<sub>2</sub> nanostructures

### 132 **2.3. Characterization**

133 The composition and crystalline arrays of prepared nanostructures were analyzed by using  
 134 X-ray diffraction (XRD) instrument by RIGAKU TTR at accelerating rate of 45 kV and current  
 135 of 45 mA with intensity of Cu K $\alpha$  radiation ( $\lambda=0.15406$  nm). The morphology was analyzed  
 136 through scanning electron microscopy (SEM) instrument by JEOL JSM-6380LV with operating  
 137 voltage of 20kV. High resolution transmission electron microscopy (HRTEM) instrument by FEI  
 138 TECHNAI G2 (containing a Schottky emitter functioning at 200kV) was applied for further  
 139 morphological characteristics in detail. Chemical attachment of materials was analyzed by X-ray  
 140 photoelectron spectroscopy (XPS) by Perkin Elmer PH 5100 XPS X-ray photoelectron  
 141 spectrometer system. Before deconvolution by CasaXPS, the spectra have been calibrated to C1s  
 142 at 285 eV. The background was a Shirley curve and for the XPS features, Voigt curves were  
 143 used. The Fourier transform infra-red (FTIR) instrument by PerkinElmer was applied for  
 144 understanding the chemical bonding features of PdO@CoSe<sub>2</sub> composites. UV aging test chamber  
 145 model no NKHS-UV was used with set parameters such as irradiation intensity of 0-  
 146 2.0W/m<sup>2</sup>/340 nm, UV wavelength range 290-400 nm, and lamp power of L=1200/40W/8pcs  
 147 during synthesis process.

### 148 **2.4. Electrochemical measurement**

149 Various electrochemical measurements were performed in 1.0M potassium hydroxide (KOH)  
 150 solution using potentiostat by VERSASTAT4-500, including linear sweep voltammetry (LSV),

151 electrochemical impedance spectroscopy (EIS), cyclic voltammetry (CV), and  
152 chronopotentiometry. Various electrochemical tests were performed using a three-electrode cell  
153 system with a modified glassy carbon electrode (GCE) as working electrode, a silver-silver  
154 chloride (Ag/AgCl) filled with 3 M potassium chloride (KCl) solution as the reference electrode,  
155 and a platinum wire as the counter electrode. Dissolving or 5 mg of each prepared catalyst (CSPd  
156 material) in 10 mL of DW and 0.1 mL of 5 % Nafion solution yielded the necessary catalytically  
157 material ink. The intended electro-catalytical slurry was based on four separate elements: pure  
158 CoSe<sub>2</sub>, PdO@CoSe<sub>2</sub>composites, and ruthenium oxide (RuO<sub>2</sub>). Before testing, a homogeneous  
159 slurry was obtained by continuously stirring in an ultrasonic bath for 20-30 minutes. Each  
160 catalyst was dropped with 5 μL onto the cleaned GCE surface (with 3 mm contact area) and  
161 dried at room temperature using an air blower. The mass of catalyst deposited onto GCE  
162 working electrode was determined to be roughly 0.2 mg. First LSV was used to examine the  
163 polarization curves for water oxidation. The EIS was used to examine the charge transfer  
164 resistance for each catalyst, with experimental conditions of sweeping frequency ranging from  
165 100 kHz to 0.1 Hz, a sinusoidal potential of 5 mV, and 1.45 V versus RHE (water oxidation  
166 onset potential). The EIS raw data was simulated by Z-view software. The durability of the as-  
167 prepared catalyst was tested for 48h at three different current densities of 20, 40, and 60 mA/cm<sup>2</sup>.  
168 The electrochemical active surface area (ECSA) was estimated non-faradic zone of CV curves  
169 obtained at various scan rates. The Nernst equation was used to report Ag-AgCl reference  
170 potential into reversible hydrogen electrode (RHE) potential

$$E_{RHE} = E_{Ag/AgCl} + 0.059 \text{ pH} + E_{Ag/AgCl}^{\circ}$$

171 Where  $E_{Ag/AgCl}^{\circ}$  is 0.2412 and overpotential ( $\eta$ ) is received by subtracting onset  
172 thermodynamic potential of 1.23 V for water splitting system.

$$173 \quad \text{Overpotential } (\eta) = \text{Onset potential } (E_{RHE}) \text{ V} - 1.23 \text{ V}$$

174 However, the Tafel slope was calculated by using Tafel equation.

$$175 \quad \eta = b \log j + a$$

176 Where  $\eta$  is overpotential,  $b$  is Tafel slope and  $j$  is current density.

### 177 **3. Results and discussion**



178            ***3.1. Crystal arrays, morphology, chemical composition and surface analysis of as***  
179            ***prepared PdO@CoSe<sub>2</sub>composites***

180            The powder X-ray diffraction (XRD) patterns were collected to investigate the  
181 crystallographic perspectives of several electro-catalytical materials, including pure cobalt  
182 selenide (CoSe<sub>2</sub>) and their composites with palladium oxide (PdO) labeled as CSPd-1, CSPd-2,  
183 and CCSPd-3. Based on the JCPDS 00-010-0409 reference card number, pure CoSe<sub>2</sub>  
184 demonstrated a cubic crystal structure, confirming successful synthesis (Fig. 1a). Furthermore,  
185 several composites of CoSe<sub>2</sub> with PdO exhibited similar cubic diffraction patterns based on the  
186 reference card number (JCPDS: 0303-065-5065). As shown by the card number (JCPDS: 03-  
187 065-5065), PdO is successfully doped in a cubic phase as evidenced by the reflections of PdO. In  
188 Fig. 1, a magnified view shows peak shifting that can be seen clearly on the right side. CoSe<sub>2</sub>  
189 nanostructures were also amended with PdO nanoparticles, which changed lattice positions and  
190 introduced additional stresses (compressive) as previously shown<sup>44, 45</sup>. As a result of stress, the  
191 position of the lattice (111) has changed kinetically which is red highlighted and clearly shown  
192 with magnification on the right side of Fig. 1. Moreover, HRTEM calculations of lattice fringes  
193 were used to validate diffraction patterns. It was not found that the composite systems contained  
194 any further peaks or other impurities based on the results of XRD analysis.

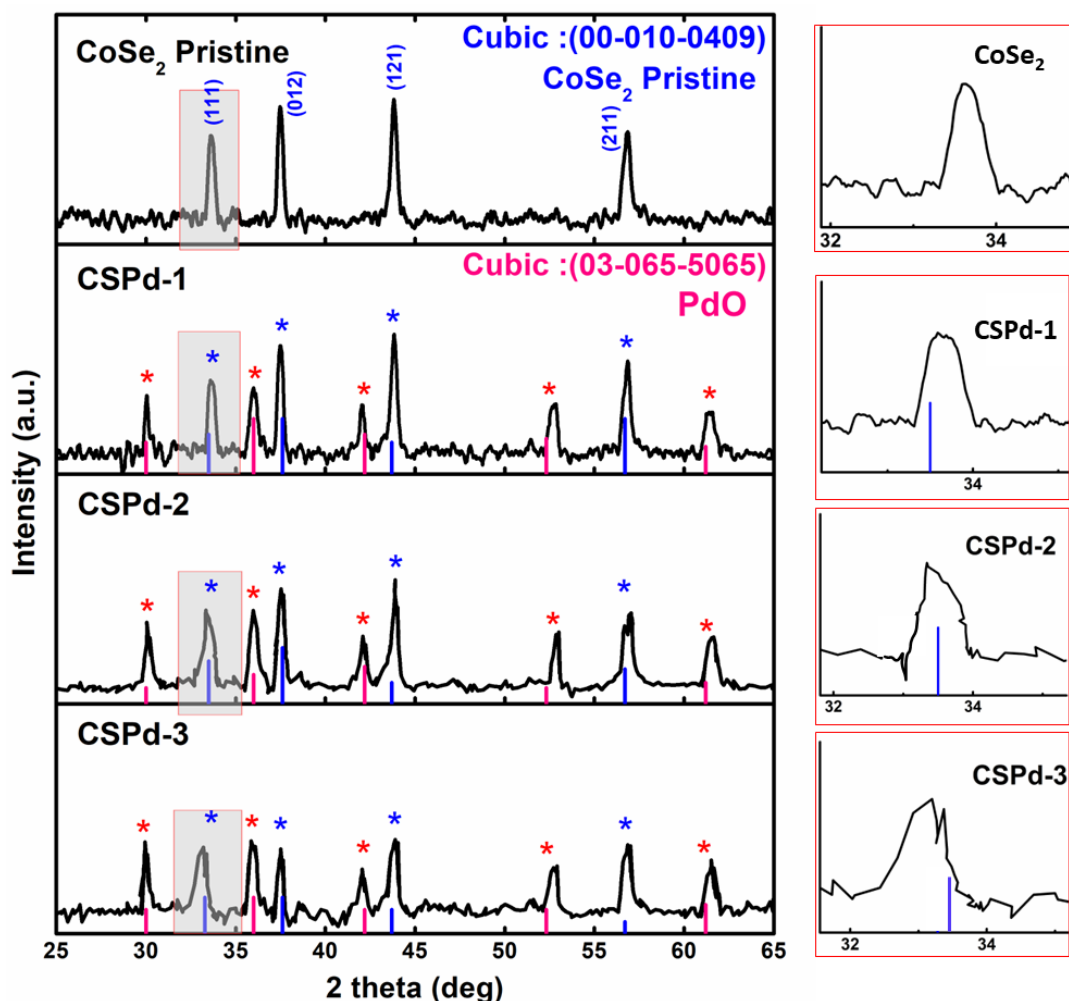


**Fig. 1** X-ray diffraction patterns of various samples such as pure and CoSe<sub>2</sub>, CSPd-1, CSPd-2 and CSPd-3 composites

195 We examined the morphologies of pristine CoSe<sub>2</sub> and its composites with PdO  
 196 nanoparticles by SEM imaging and elucidated their elemental compositions by EDS spectra, Fig.  
 197 2.

198 The CoSe<sub>2</sub> nanostructures were characterized with sharp edges topical surface shapes  
 199 and a lumpy morphology<sup>46, 47</sup>. Aside from the physical morphology of CoSe<sub>2</sub>, its chemical  
 200 composition has been confirmed by EDS spectrum as shown from right side of Fig. 2. (a) and  
 201 only Co and Se elements were identified. Additionally, the as-prepared composite nanostructures  
 202 had slightly heterogeneous morphologies characterized by sharp edges aggregating with PdO

203 nanoparticles (Fig. 2 (b), (c) and (d), respectively<sup>48, 49</sup>. An EDS analysis of composite systems  
204 revealed that Pd was present along with Co and Se elements in very small quantities. We have  
205 performed an elemental mapping to describe the distribution of various elements in pure CoSe<sub>2</sub>  
206 and composite systems as shown in supplementary figures (S1 and S2). According to both SEM  
207 and EDS analysis, PdO has successfully been doped on CoSe<sub>2</sub> and the morphology has been  
208 slightly changed as evidenced by the presence of Co, Se, and Pd elements. TEM analysis was  
209 also performed to obtain localized information at the atomic level for pure CoSe<sub>2</sub> and its  
210 composite samples like CSPd-1, CSPd-2, and CSPd-3 for viewing and understanding the lattice  
211 fringes within the samples. On the right side of Fig. 3, Fast Fourier transform (FFT) images are  
212 shown for each sample. As shown in Fig. 3a, pure CoSe<sub>2</sub> nanostructures have lumpy shapes and  
213 are highly consistent with SEM results. CoSe<sub>2</sub> was found to have a d- spacing of 0.32 nm in the  
214 pure sample, as previously demonstrated<sup>50, 51</sup>.

215 The morphologies of as-prepared composite materials such as CSPd-1, CSPd-2 and  
216 CSPd-3 are depicted in Fig. 3 (b), (c) and (d) along with d-spacing values respectively. The  
217 FFT analysis has shown the d-spacing values as 0.33, 0.308, and 0.208 nm for SPd-1, CSPd-2  
218 and CSPd-3<sup>52</sup>. The d- spacing values suggest that the materials are well defined by the  
219 nanostructured phase and with excellent crystalline qualities<sup>53, 54</sup>.

220 The chemical state and surface composition of various materials have been examined  
221 using X-ray photoelectron spectroscopy (XPS) as shown in Fig. 4. The Co2*p* photoelectron  
222 signals of pure CoSe<sub>2</sub> can be seen in Fig. 4(a). It shows four doublets corresponding to Co 2*p*<sub>3/2</sub>  
223 and Co 2*p*<sub>1/2</sub> contributions and the relevant spectra matched with the previously reported cobalt  
224 spinel phase<sup>47, 55</sup>. However, the peak at 779.46 eV corresponds to Co<sup>3+</sup>, peak at 780.87 eV is in-  
225 tune-with Co<sup>2+</sup> and the signal at 785.51 eV represents Co<sup>2+</sup> in Co(OH)<sub>2</sub><sup>35</sup>. As shown in Fig. 4(c),  
226 the binding energy between the two materials has somewhat altered. As with Fig. 4(b) and (d),  
227 the Se3*d* has two high binding energy contributions at 60.11 eV and 62.00 eV coming from  
228 selenium-oxygen bonds probably located at the catalyst surface<sup>56</sup>. Additionally, two peaks at  
229 54.60 eV and 56.29 eV correspond to Se3*d*<sub>3/2</sub> and 55.45 eV and 57.22 eV correspond to Se3*d*<sub>5/2</sub>  
230 feature. These latter are due to selenium-metal bonding structure as well<sup>56</sup>. For CSPd-2, Co2*p*,  
231 Se3*d* and Pd3*d* are shown in figures 4c, 4d and 4e. Similarly, to CoSe<sub>2</sub> (Fig. 4a), Co2*p* of CSPd-  
232 2 shows Co<sup>3+</sup>, Co<sup>2+</sup> and hydroxylated cobalt contributions at around 779.28 eV, 780.27 eV and

233 785.04 eV (Fig. 4c). Regarding Se3d feature of CSPd-2 (Fig. 4d), the binding energy of Se-metal  
234 contributions are located at 54.88 eV and 56.13 eV for Se3d<sub>3/2</sub> and 55.33 eV and 56.44 eV for  
235 Se3d<sub>5/2</sub> feature. The higher binding energy contributions at 60.20 eV and 62.34 eV are assigned  
236 to selenium-oxygen bonds. Pd3d peaks have been observed from sample CSPd-2 which revealed  
237 the two main peaks at 337.24 eV and 342.53 eV, can be assigned to Pd3d<sub>5/2</sub> and Pd3d<sub>3/2</sub>  
238 respectively<sup>57</sup>, as shown Fig. S3(a). Furthermore, supplementary Fig. S3(b) illustrates the XPS  
239 survey spectrum of CSPd-2.

240 The Fourier transform infrared (FTIR) of several samples can be seen in Supplementary  
241 Fig. (S4). Using this technique, it is possible to confirm the presence of characteristic vibrations  
242 and functional groups in the samples. In line with related research, the broader bands observed at  
243 3300-3400 cm<sup>-1</sup> and 1400 to 1500 cm<sup>-1</sup> are likely caused by OH<sup>-</sup> stretching and adsorbed water  
244 molecules at the surface of samples due to moisture absorption<sup>58</sup>. The fundamental characteristic  
245 vibrational modes of Co-Se bonding could be assigned to bands ranging from 500 to 900 cm<sup>-1</sup><sup>59</sup>.  
246 The parallel cCoSe2 nanostructures show decreased band structure due to cobalt and selenium  
247 vibrating at different frequencies<sup>60</sup>. As a result of the presence of PdO into CoSe<sub>2</sub>, the broader  
248 peak at 875 cm<sup>-1</sup> has been lowered, and a little hump can be seen in CSPd-3 as a result of Pd<sup>61</sup>.  
249 An analysis of the FTIR spectrum confirmed the development of pure CoSe<sub>2</sub> and composite  
250 nanostructures.

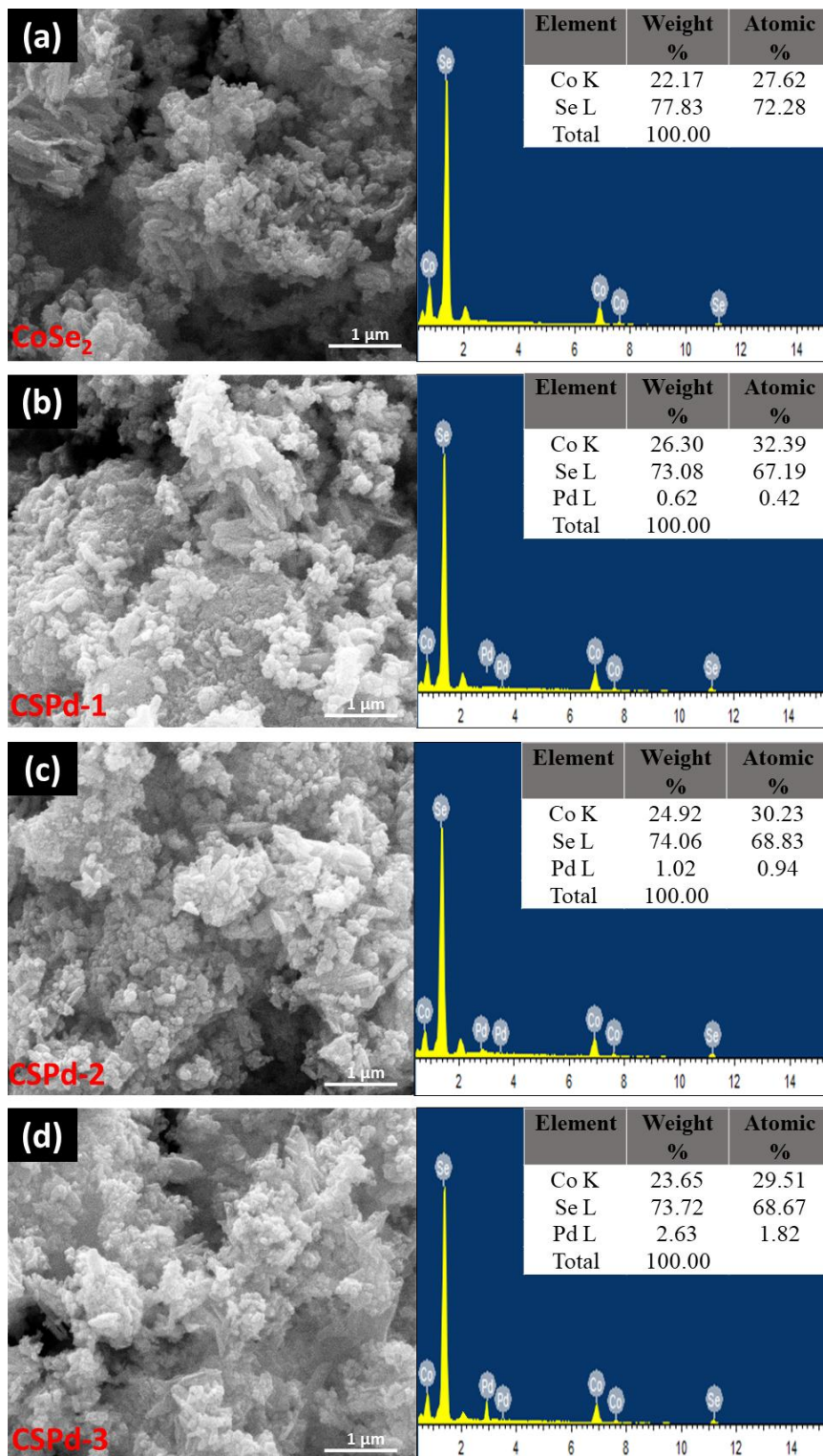


**Fig. 2** SEM and EDS spectra of different nanostructures (a) CoSe<sub>2</sub> (b) CSPd-1 (c) CSPd-2 and (d) CSPd-3

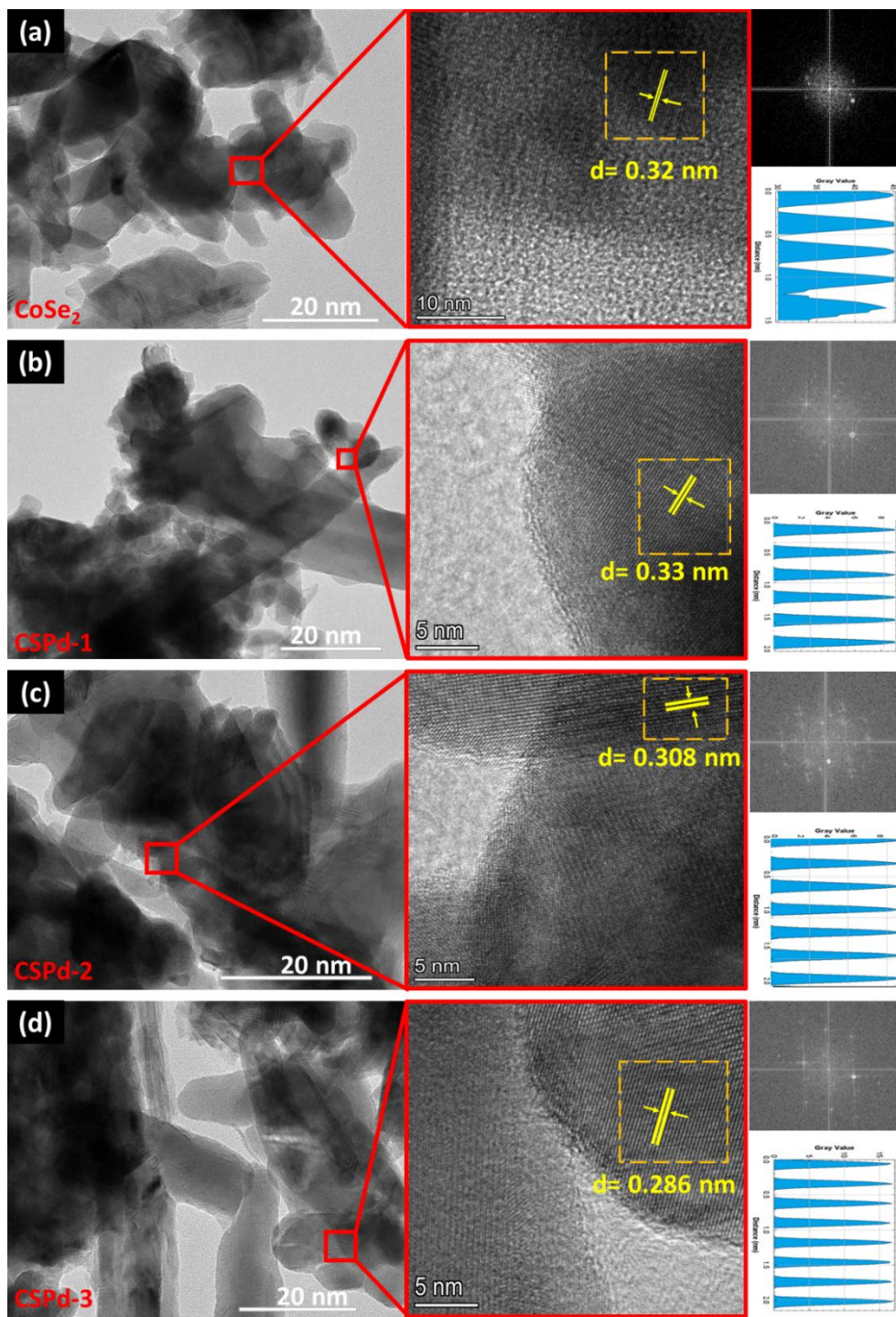


**Fig. 3** HRTEM images of various nanostructures along with their FFT and lattice fringes calculation (a) CoSe<sub>2</sub> (b) CSPd-1 (c) CSPd-2 and (d) CSPd-3



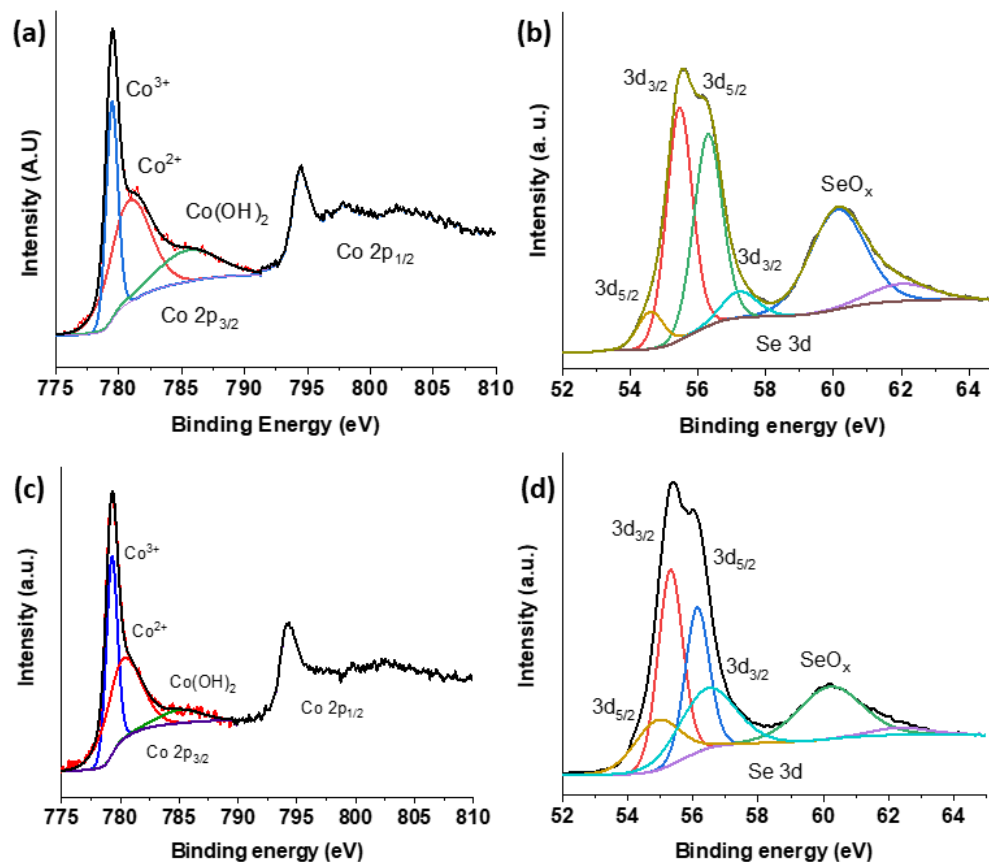


**Fig. 4** XPS spectra of various nanostructures CoSe<sub>2</sub>; (a) Co2p (b) Se3d and CSPd-2; (c) Co2p (d) Se3d

253

254

### 3.2. Electrochemical performance of PdO@ CoSe<sub>2</sub> for water oxidation

255

256

257

258

259

260

261

262

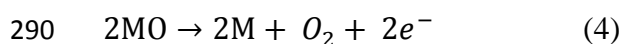
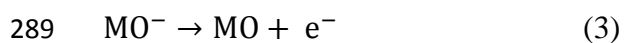
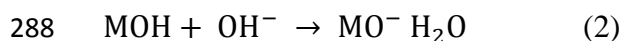
263

The electrochemical half-cell characterization for water oxidation was carried with LSV at 2 mV/s polarization curves for pristine CoSe<sub>2</sub>, CSPd-1, CSPd-2, and CSPd-3 composites, and Ruthenium Oxide (RuO<sub>2</sub>) in 1M KOH as shown in Fig. 5a. The measured overpotentials for pure CoSe<sub>2</sub>, CSPd-1, CSPd-2, and CSPd-3, are 350, 320, 260, and 290 mV at 20 mA/cm<sup>2</sup> respectively. The pure CoSe<sub>2</sub> sample has exhibited large overpotential, indicating that the material has capability to show activity for OER reaction, however its high energy barrier is the main challenge due to its few active sites, and poorly organized surface properties. Whereas the composite CSPd-1 has described relatively lower energy barrier for OER and the composite CSPd-2 has the lowest overpotential of 260 mV at 20 mA/cm<sup>2</sup>, confirming that doping of few

264 amounts of PdO onto CoSe<sub>2</sub> can significantly reduce the energy barrier during water oxidation.  
265 Furthermore, the agglomeration of PdO nanoparticles for CSPd-3 has decreased the activity of  
266 composite system and indicating that the certain amount of PdO is sufficient to accelerate the  
267 reaction kinetics and efficiency of materials towards electrochemical water splitting as shown in  
268 Fig. 5a. For better visualization bar graph of overpotential for various materials is enclosed in  
269 Fig. 5b. The ruthenium oxide (RuO<sub>2</sub>) has been investigated with lower overpotential and it is  
270 being a state of art catalyst has the limitation of high cost and rare abundance, however  
271 heterostructure CSPd-2 has closely assigned overpotential and it could be used as an alternative  
272 material for large scale production of oxygen gas as a green fuel and for full exploitation of  
273 hydrogen form water splitting. The lower energy demand based on the CSPd-2 is attributed to  
274 high density of active sites, fast charge transport, defects in the crystal structure, large surface  
275 area due to nanoscale dimension, and favorable surface science owing to multi d orbital  
276 configuration.

277 By using the Tafel slope equation as the rate-determining step for the OER mechanism  
278 was evaluated from the linear region of LSV and the calculation was made as previous reported  
279 work<sup>62</sup>, as shown in the Fig. 5(c). Particularly compared to pristine CoSe<sub>2</sub> and other composite  
280 materials like CSPd-2 has low Tafel slope value of 57 mVdec<sup>-1</sup> and its close to noble metal RuO<sub>2</sub>  
281 with a Tafel slope value of 52 mVdec<sup>-1</sup>, suggesting that the proposed materials have almost swift  
282 reaction kinetics as exhibited by noble metal material. The relative lowering of Tafel slope  
283 values of tested materials were found the in the order RuO<sub>2</sub> < CSPd-2 < CSPd-3 < CSPd-1 <  
284 CoSe<sub>2</sub> as enclosed in Fig. 5c.

285 The water oxidation is accompanied by the involvement of four electron transfer process and  
286 general steps involved in the alkaline reaction are described by the following main steps:





291 Theoretical Tafel analysis for the estimation of water oxidation reaction mechanism is associated  
292 with the Tafel values of 120, 60, 40, and 15 mV/dec. The proposed study is favored by the step 2  
293 and it could, be considered as rate limiting step for water oxidation under alkaline conditions <sup>63-</sup>  
294 <sup>66</sup>.

295 It is interesting to note that electrochemical performance for as-prepared material is  
296 strongly connected to the durability of material for long term reaction. Hence, the  
297 chronopotentiometry experiment was performed to evaluate stability of as prepared CDPd-2  
298 composite material for 48 h at various current densities such as 20, 40, and 60 mA/cm<sup>2</sup>, as shown  
299 in Fig. 5d. It is obvious that the potential drop for the set period of durability was negligible and  
300 the CSPd-2 material has an excellent durability as shown in Fig. 5d and the performance is close  
301 to the recently reported nonprecious materials <sup>67, 68</sup>. Additionally, the stability of CSPd-2 was  
302 investigated after the durability test using LSV polarization curves before and after the stability  
303 test as shown in Fig. 5e. The observations of stability by LSV, are highly encouraging that the  
304 material transformation and the change in the surface properties remained inactive, with  
305 outstanding stability. The confirmation of material chemical transformation, the post SEM and  
306 EDS analysis were performed and they have shown negligible chemical change in the  
307 composition and morphological aspects, after chronopotentiometry as depicted in supplementary  
308 Fig. (S5).

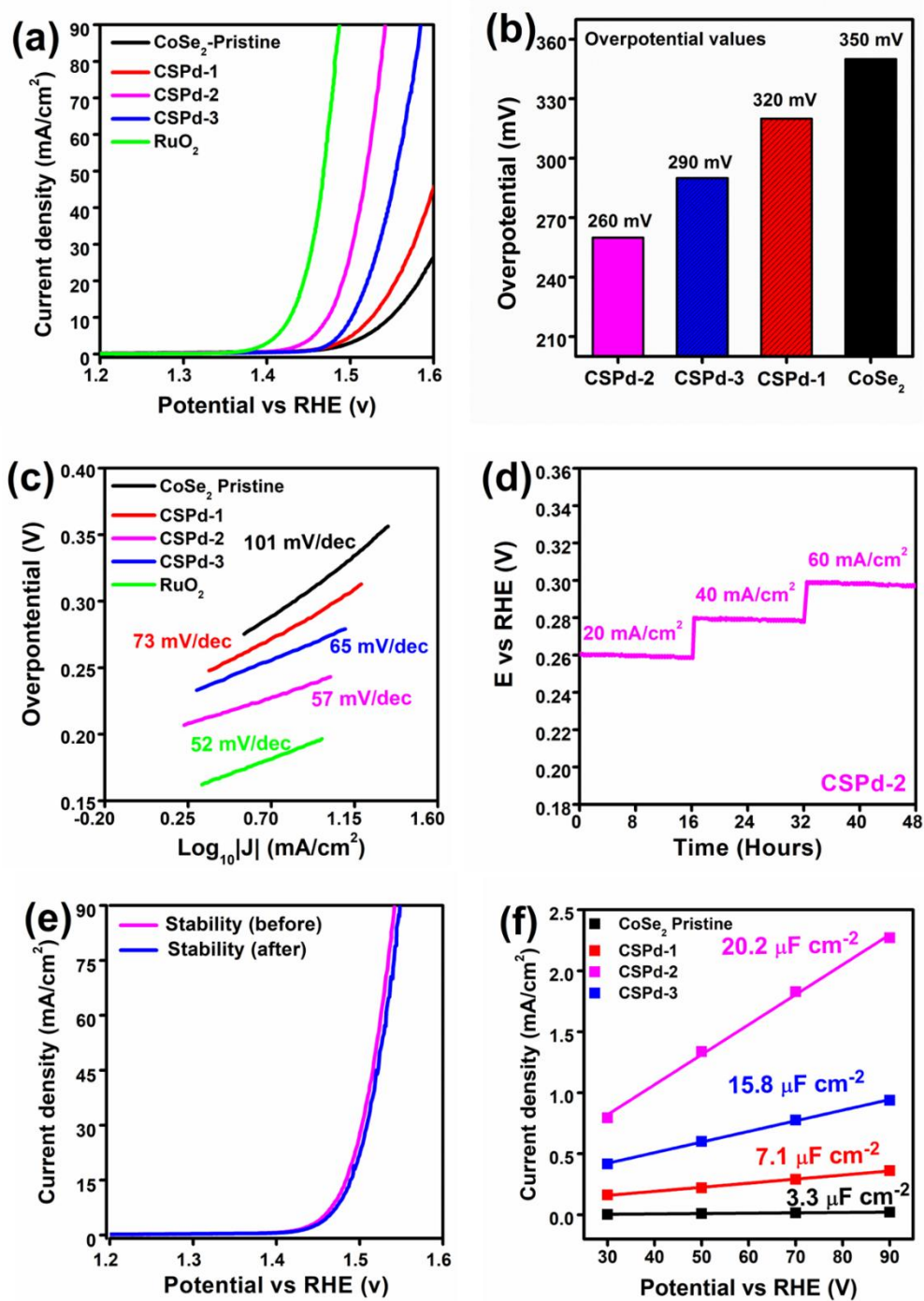


**Fig. 5** (a) LSV curves of various nanostructures including CoSe<sub>2</sub>, CSPd-1, CSPd-2 and CSPd-3 with reference of RuO<sub>2</sub> at 20  $\text{mA}/\text{cm}^2$  (b) Histogram of overpotential values for different catalysts (c) Tafel slope values of various materials (d) Chronopotentiometry of as-prepared

catalyst at different current densities such as 20, 40 and 60 mA/cm<sup>2</sup> (e) Durability test of CSPd-2 before and after chronopotentiometry test (f) Double layer capacitance (C<sub>dl</sub>) values of various catalysts, calculated at various scan rates from CV curves.

309 To examine superior OER performance, we used electrochemical active surface area  
310 (ECSA) for comparing active sites by employing non-faradaic area of CV curves at different  
311 scan rat, as shown in supplement Fig. (S6) by using the following equation.

312 
$$ECSA = C_{dl} / C_s$$

313 where C<sub>s</sub> is 0.04 mF/cm<sup>2</sup> for KOH electrolyte<sup>69, 70</sup>. The C<sub>dl</sub> (double layer capacitance) is  
314 plotted as capability of sweep scan rate and linear fitting was used to determine the slope  
315 value<sup>71,72</sup>, as given in Fig. 5(f). The calculated value of ECSA for CSPd-2 is 310 cm<sup>2</sup> which is  
316 higher value than the other materials, thus it is one of the factors for the improvement of the  
317 performance of towards water oxidation.

318 The EIS is a necessary step in analyzing the charge transfer mechanism between  
319 electrolyte and working electrode. The Z-view software was used to simulate the raw data of EIS  
320 using an equivalent circuit as inset shown in Fig. 6 Nyquist plots were used to estimate the  
321 charge transfer resistance (R<sub>ct</sub>) values of each material<sup>73</sup>, as enclosed in Fig. 6(a). The Bode  
322 plots have given phase features at different frequencies, shown in Fig. 6(b). Additionally, Fig.  
323 6(c) shows the phase angle within bode plots 65°, 42°, 24° and 19° for CoSe<sub>2</sub>, CSPd-1, CSPd-3  
324 and CSP-2 accordingly.

325 The R<sub>ct</sub> (charge transfer resistance) values for pristine CoSe<sub>2</sub>, CSPd-1, CSPd-2 and CSPd-  
326 3 were calculated as 395, 115, 47 and 87 Ω respectively which are well supported by the recently  
327 reported EIS results<sup>74-76</sup>. The lower charge transfer value of CSPd-2 favored quick charge  
328 transfer at the interface of electrolyte and the electrode for favorable water oxidation.

329

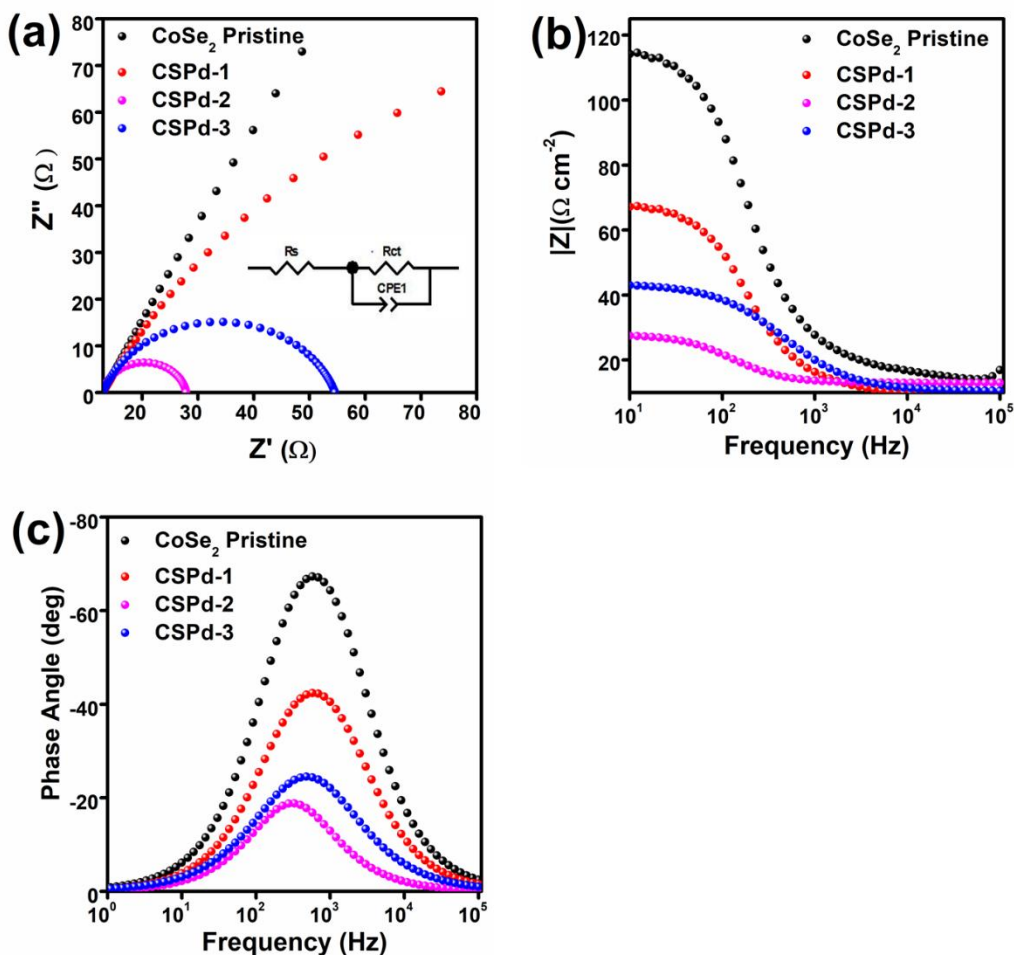


**Fig. 6** (a) Corresponding Nyquist plots of dissimilar materials (b) and (c) Bode plots

330 The summary of obtained electrochemical results from LSV, ECSA, and EIS analysis is  
 331 given in Table 1. It is obvious that the electrochemical performance of CSPd-2 composite is  
 332 superior to many the tested materials in the proposed study, hence it can be used an effective  
 333 material energy conversion and energy storage systems. Furthermore, the comparative analysis  
 334 in terms Tafel slope and lower overpotential of CSPd-2 was compared with previously reported  
 335 electrocatalysts, as shown in the supplementary (Table S1). The CSPd-2 composite system has  
 336 either superior or equal performance to the recently reported works in terms of low  
 337 overpotential and Tafel slope. After adding the desired few amounts of PdO as contributing  
 338 factor for the enhancement of water oxidation performance onto CoSe<sub>2</sub> is significantly proven as  
 339 a promoter.

**Table 1.** Electrochemical Features of various electrocatalysts.

| <b>Catalyst</b>                  | <b>Calculation by LSV</b> | <b>Calculation by EIS</b>  |                          | <b>Calculation by CV</b>      |                                     |
|----------------------------------|---------------------------|----------------------------|--------------------------|-------------------------------|-------------------------------------|
|                                  | Tafel Slope               | Charge Transfer Resistance | Double Layer Capacitance | Double Layer Capacitance      | Electrochemical Active Surface Area |
|                                  | $\frac{B}{mV/Dec}$        | $\frac{R_{ct}}{\Omega}$    | $\frac{CPE_{dl}}{mF}$    | $\frac{C_{dl}}{(\mu F/cm^2)}$ | $\frac{ECSA}{cm^2}$                 |
| <b>Pristine CoSe<sub>2</sub></b> | 101                       | 395                        | 0.04                     | 3.8                           | 95                                  |
| <b>CSPd-1</b>                    | 73                        | 115                        | 0.095                    | 6.9                           | 172                                 |
| <b>CSPd-2</b>                    | 57                        | 47                         | 0.37                     | 12.8                          | 320                                 |
| <b>CSPd-3</b>                    | 65                        | 87                         | 0.21                     | 9.2                           | 230                                 |

#### 342 4. Conclusion

343 In summary, we attempted to doping the PdO onto CoSe<sub>2</sub> nanostructures prepared via wet  
 344 chemical reduction using UV light. As demonstrated by SEM and HRTEM analysis, the  
 345 morphology is heterogeneous, while the crystalline properties are excellent. CoSe<sub>2</sub>  
 346 nanostructures were found to have PdO on their surfaces based on XRD and XPS results. The  
 347 electrochemical properties of the as-prepared material towards water oxidation with low  
 348 overpotential of 260 mV at a current density of 20 mA/cm<sup>2</sup> and a low Tafel Slope value of 57  
 349 mV/dec was observed for the CSPd-2 composite system. In addition, CSPd-2 demonstrated low  
 350 charge transfer resistance R<sub>ct</sub> of 47 Ω. A 48-hour durability period further validated the  
 351 electrocatalytic properties of CSPd-2. The evaluated performance of CSPd-2 composite sample  
 352 using a small quantity of PdO played a dynamic role in the development efficient electrocatalyst  
 353 and it has high window to apply for wide range of electrochemical applications such as batteries,  
 354 water electrolysis, and supercapacitors.

355

#### 356 Acknowledgement

357 B.V. thank the platform “Microscopies, Microprobes and Metallography (3M)” (Institut Jean  
 358 Lamour, IJL, Nancy, France) for access to SEM facilities and F. Alnjiman for his valuable help.  
 359 We also acknowledge partial funding of the Ajman University, Grant ID: DGSR Ref: 2022-IRG-  
 360 HBS-5, and we would like to thank the platform of National Natural Science Foundation of  
 361 China (NSFC 51402065 and 51603053).

362 **Author contribution**

363 Abdul Hanan, has prepared the materials, did electrocatalysis and wrote part of manuscript.

364 Muhammad Yameen Solangi, did partial physical characterization testing.

365 Abdul Jaleel Laghari, did Tafel analysis.

366 Aqeel Ahmed Shah, electrochemical active surface analysis and involved in the discussion.

367 Umair Aftab, did impedance experiment and wrote the discussion.

368 Muhammad Ishaque Abro, partially supervised the manuscript and supported the electrochemical  
369 testing.

370 Muhammad Nazim Lakhan, analyzed the XPS results.

371 Irfan Ali, did all graphic materials including graphical abstract and schemes.

372 Elmuez A. Dawi, theoretical interpretation, preparation of the manuscript.

373 Abd Al Karim Haj Ismail, theoretical interpretation, preparation of the manuscript.

374 Elfatih Mustafa, preparation of the manuscript.

375 Brigitte Vigolo analyzed XPS results and edited the draft of manuscript

376 Aneela Tahira, analyzed the SEM and TEM results.

377 Zafar Hussain Ibupoto, provided the hypothesis and overall supervise the work and involved  
378 manuscript.

379 **Data availability statement**

380 Data available in article supplementary material.

381 **Conflict of interest**

382 All authors declare no conflict of interest in this research work.

383

384 **References**

- 385 1. C. Hu, Y. Xiao, Y. Zou and L. Dai, *Electrochemical Energy Reviews*, 2018, **1**, 84-112.  
386 2. *Nature Reviews Chemistry*, 2018, **2**, 0125.  
387 3. S. Ghosh and R. N. Basu, *Nanoscale*, 2018, **10**, 11241-11280.  
388 4. D. Guo, H. Kang, P. Wei, Y. Yang, Z. Hao, Q. Zhang and L. Liu, *CrystEngComm*, 2020, **22**,  
389 4317-4323.  
390 5. S. Ponnada, M. S. Kiai, D. B. Gorle, R. S. C. Bose, V. Rajagopal, B. Saini, M. Kathiresan, A.  
391 Nowduri, R. Singhal, F. Marken, M. A. Kulandainathan, K. K. Nanda and R. K. Sharma,  
392 *Catalysis Science & Technology*, 2022, **12**, 4413-4441.  
393 6. S. L. Pasarakonda, S. Ponnada, D. B. Gorle, R. S. Chandra Bose, A. Palariya, M. S. Kiai, H. B.  
394 Gandham, M. Kathiresan, R. K. Sharma and A. Nowduri, *New Journal of Chemistry*, 2023, DOI:  
395 10.1039/D2NJ04648B.  
396 7. A. Shankar, R. Elakkiya and G. Maduraiveeran, *New Journal of Chemistry*, 2020, **44**, 5071-5078.  
397 8. H. Eidsvåg, S. Bentouba, P. Vajeeston, S. Yohi and D. Velauthapillai, *Molecules*, 2021, **26**, 1687.  
398 9. M. Ahmed, M. N. Lakhan, A. Hanan, R. Ahmed, A. H. Shar, I. Ali, S. Mahesar, M. A. Latif, A.  
399 Muhammad and M. A. Usto.  
400 10. S. Mishra, P. Yogi, P. R. Sagdeo and R. Kumar, *ACS Applied Energy Materials*, 2018, **1**, 790-  
401 798.  
402 11. A. QayoomMugheri, AneelaTahira, U. Aftab, M. IshaqAbro, S. R. Chaudhry, L. Amaral and Z.  
403 H. Ibupoto, *Electrochimica Acta*, 2019, **306**, 9-17.  
404 12. A. Sajeev, V. K. Mariappan, D. Kesavan, K. Krishnamoorthy and S.-J. Kim, *Materials Advances*,  
405 2021, **2**, 455-463.  
406 13. M. Łuba, T. Mikołajczyk, M. Kuczyński, B. Pierożyński and I. M. Kowalski, *Catalysts*, 2021, **11**,  
407 468.  
408 14. S. M. Galani, A. Mondal, D. N. Srivastava and A. B. Panda, *International Journal of Hydrogen*  
409 *Energy*, 2020, **45**, 18635-18644.  
410 15. W. Luo, J. Gan, Z. Huang, W. Chen, G. Qian, X. Zhou and X. Duan, *Frontiers in Materials*,  
411 2019, **6**.  
412 16. C. Li and J.-B. Baek, *ACS Omega*, 2020, **5**, 31-40.  
413 17. X. Ren, Q. Lv, L. Liu, B. Liu, Y. Wang, A. Liu and G. Wu, *Sustainable Energy & Fuels*, 2020, **4**,  
414 15-30.  
415 18. J. Peng, Y. Chen, K. Wang, Z. Tang and S. Chen, *International Journal of Hydrogen Energy*,  
416 2020, **45**, 18840-18849.  
417 19. R. K. Hona, S. B. Karki and F. Ramezanipour, *ACS Sustainable Chemistry & Engineering*, 2020,  
418 **8**, 11549-11557.  
419 20. M. Y. Solangi, A. H. Samo, A. J. Laghari, U. Aftab, M. I. Abro and M. I. J. S. I. J. o. E. T. Irfan,  
420 2022, **5**, 32-40.  
421 21. Y. Xue, S. Sun, Q. Wang, Z. Dong and Z. Liu, *Journal of Materials Chemistry A*, 2018, **6**, 10595-  
422 10626.  
423 22. Y. Zhu, Q. Lin, Y. Zhong, H. A. Tahini, Z. Shao and H. Wang, *Energy & Environmental Science*,  
424 2020, **13**, 3361-3392.  
425 23. M. Wang, L. Zhang, Y. He and H. Zhu, *Journal of Materials Chemistry A*, 2021, **9**, 5320-5363.  
426 24. Y.-N. Zhou, Y.-R. Zhu, X.-Y. Chen, B. Dong, Q.-Z. Li and Y.-M. Chai, *Journal of Alloys and*  
427 *Compounds*, 2021, **852**, 156810.  
428 25. H. Du, R.-M. Kong, X. Guo, F. Qu and J. Li, *Nanoscale*, 2018, **10**, 21617-21624.  
429 26. P. Li and H. C. Zeng, *ACS Applied Materials & Interfaces*, 2019, **11**, 46825-46838.  
430 27. X. Xia, L. Wang, N. Sui, V. L. Colvin and W. W. Yu, *Nanoscale*, 2020, **12**, 12249-12262.  
431 28. Y. Xue, G. Ma, X. Wang, M. Jin, E. M. Akinoglu, D. Luo and L. Shui, *ACS Applied Materials &*  
432 *Interfaces*, 2021, **13**, 7334-7342.  
433 29. M. Jahan, Z. L. Liu and K. P. Loh, *Advanced Functional Materials*, 2013, **23**, 5363-5372.

- 434 30. G. Mei, H. F. Liang, B. B. Wei, H. H. Shi, F. W. Ming, X. Xu and Z. C. Wang, *Electrochimica Acta*, 2018, **290**, 82-89.
- 435
- 436 31. Z. W. Fang, L. L. Peng, H. F. Lv, Y. Zhu, C. S. Yan, S. Q. Wang, P. Kalyani, X. J. Wu and G. H. Yu, *Acs Nano*, 2017, **11**, 9550-9557.
- 437
- 438 32. F. O. Boakye, Y. Li, K. A. Owusu, I. S. Amiin, Y. P. Cheng and H. N. Zhang, *Materials Chemistry and Physics*, 2022, **275**.
- 439
- 440 33. I. M. Abdullahi, J. Masud, P.-C. Ioannou, E. Ferentinos, P. Kyritsis and M. Nath, *Molecules*, 2021, **26**, 945.
- 441
- 442 34. J. Masud, A. T. Swesi, W. P. Liyanage and M. Nath, *ACS Appl Mater Interfaces*, 2016, **8**, 17292-17302.
- 443
- 444 35. L. Xia, H. Song, X. Li, X. Zhang, B. Gao, Y. Zheng, K. Huo and P. K. Chu, *Frontiers in Chemistry*, 2020, **8**.
- 445
- 446 36. J. Sun, J. Li, Z. Li, X. Hu, H. Bai and X. Meng, *ACS Sustainable Chemistry & Engineering*, 2022, **10**, 4022-4030.
- 447
- 448 37. X. Zheng, J. Zhang, J. Wang, Z. Zhang, W. Hu and Y. Han, *Science China Materials*, 2020, **63**, 347-355.
- 449
- 450 38. X. Cao, J. E. Medvedeva and M. Nath, *ACS Applied Energy Materials*, 2020, **3**, 3092-3103.
- 451 39. Z. Feng, B. Gao, L. Wang, H. Zhang, P. Lu and P. Xing, *Journal of The Electrochemical Society*, 2020, **167**, 134501.
- 452
- 453 40. L. Shreenivasa, S. Ashoka, K. Yogesh, A. Syed, N. Marraiki and P. S. Adarakatti, *Solid State Sciences*, 2022, **124**.
- 454
- 455 41. J. Saha, S. Verma, R. Ball, C. Subramaniam and R. Murugavel, *Small*, 2020, **16**.
- 456 42. S. Saddeler, G. Bendt, S. Salamon, F. T. Haase, J. Landers, J. Timoshenko, C. Rettenmaier, H. S. Jeon, A. Bergmann, H. Wende, B. R. Cuenya and S. Schulz, *Journal of Materials Chemistry A*, 2021, **9**, 25381-25390.
- 457
- 458
- 459 43. J. X. Flores-Lasluisa, F. Huerta, D. Cazorla-Amoros and E. Morallon, *Nanomaterials*, 2020, **10**.
- 460 44. M. Y. Solangi, U. Aftab, A. Tahira, M. I. Abro, R. Mazarro, V. Morandi, A. Nafady, S. S. Medany, A. Infantes-Molina and Z. H. Ibutoto, *International Journal of Hydrogen Energy*, 2022, **47**, 3834-3845.
- 461
- 462
- 463 45. A. Nakrela, N. Benramdane, A. Bouzidi, Z. Kebbab, M. Medles and C. Mathieu, *Results in Physics*, 2016, **6**, 133-138.
- 464
- 465 46. H. Liu, K. Xiang, B. Yang, X. Xie, D. Wang, C. Zhang, Z. Liu, S. Yang, C. Liu, J. Zou and L. Chai, *Environmental Science and Pollution Research*, 2017, **24**, 14249-14258.
- 466
- 467 47. L. Zhao, J. Jia, Y. Chang, M. Jia and Z. Wen, *International Journal of Hydrogen Energy*, 2019, **44**, 22787-22795.
- 468
- 469 48. H. Wang, S. Zhang, S. Li and J. Qu, *Analytical Methods*, 2018, **10**, 1331-1338.
- 470 49. A. Zhou, R.-M. Guo, J. Zhou, Y. Dou, Y. Chen and J.-R. Li, *ACS Sustainable Chemistry & Engineering*, 2018, **6**, 2103-2111.
- 471
- 472 50. D. S. Gavhane, H. van Gog, B. Thombare, G. Lole, L. Christiaan Post, M. A. More and M. A. van Huis, *npj 2D Materials and Applications*, 2021, **5**, 24.
- 473
- 474 51. G. Zhao, P. Li, K. Rui, Y. Chen, S. X. Dou and W. Sun, *Chemistry*, 2018, **24**, 11158-11165.
- 475 52. V.-D. Le, T. C.-H. Le, V.-T. Chau, T. N.-D. Le, C.-H. Dang, T. T.-N. Vo, T. D. Nguyen and T.-D. Nguyen, *New Journal of Chemistry*, 2021, **45**, 4746-4755.
- 476
- 477 53. S. Sarkar and S. C. Peter, *Inorganic Chemistry Frontiers*, 2018, **5**, 2060-2080.
- 478 54. T. Shen, J. Zhang, K. Chen, S. Deng and D. Wang, *Energy & Fuels*, 2020, **34**, 9137-9153.
- 479 55. M. C. Biesinger, B. P. Payne, A. P. Grosvenor, L. W. M. Lau, A. R. Gerson and R. S. C. Smart, *Applied Surface Science*, 2011, **257**, 2717-2730.
- 480
- 481 56. X. Wang, Y. Xie, B. Bateer, K. Pan, X. Zhang, J. Wu and H. Fu, *ACS Sustainable Chemistry & Engineering*, 2019, **7**, 2784-2791.
- 482
- 483 57. Q.-S. Jiang, W. Li, J. Wu, W. Cheng, J. Zhu, Z. Yan, X. Wang and Y. Ju, *Journal of Materials Science: Materials in Electronics*, 2019, **30**, 9429-9437.
- 484



- 485 58. B. Jansi Rani, G. Ravi, R. Yuvakkumar, B. Saravanakumar, M. Thambidurai, C. Dang and D.  
486 Velauthapillai, *ACS omega*, 2020, **5**, 14702-14710.
- 487 59. Y. R. Zheng, M. R. Gao, Q. Gao, H. H. Li, J. Xu, Z. Y. Wu and S. H. Yu, *Small*, 2015, **11**, 182-  
488 188.
- 489 60. S. Swathi, B. J. Rani, R. Yuvakkumar, G. Ravi, E. S. Babu, M. Pannipara, A. G. Al-Sehemi and  
490 D. Velauthapillai, *Applied Nanoscience*, 2021, **11**, 1367-1378.
- 491 61. H. Mansouri-Torshizi, E. Rezaei, F. Kamranfar and M. Heidari Majd, *Advanced pharmaceutical  
492 bulletin*, 2016, **6**, 449-453.
- 493 62. T. Shinagawa, A. T. Garcia-Esparza and K. Takanabe, *Scientific Reports*, 2015, **5**, 13801.
- 494 63. A. Hanan, 2021, 2021, **11**.
- 495 64. S.-J. Huang, S. Balu, N. R. Barveen and R. Sankar, *Colloids and Surfaces A: Physicochemical  
496 and Engineering Aspects*, 2022, 130024.
- 497 65. C. Zhou, X. Han, F. Zhu, X. Zhang, Y. Lu, J. Lang, X. Cao and H. Gu, *International Journal of  
498 Hydrogen Energy*, 2022, **47**, 27775-27786.
- 499 66. A. Samo, U. Aftab, D. Cao, M. Ahmed, M. Lakhan, V. Kumar, A. Asif, A. J. D. J. o. N. Ali and  
500 Biostructures, 2022, **17**.
- 501 67. T. Reier, M. Oezaslan and P. Strasser, *ACS Catalysis*, 2012, **2**, 1765-1772.
- 502 68. J. Yu, F. A. Garcés-Pineda, J. González-Cobos, M. Peña-Díaz, C. Rogero, S. Giménez, M. C.  
503 Spadaro, J. Arbiol, S. Barja and J. R. Galán-Mascarós, *Nature Communications*, 2022, **13**, 4341.
- 504 69. T. Ingsel and R. K. Gupta, in *Nanomaterials for Electrocatalysis*, eds. T. Maiyalagan, M.  
505 Khandelwal, A. Kumar, T. A. Nguyen and G. Yasin, Elsevier, 2022, 83-111.
- 506 70. D. S. Butenko, S. Li, V. O. Kotsyubynsky, V. M. Boychuk, V. I. Dubinko, P. I. Kolkovsky, N. A.  
507 Liedienov, N. I. Klyui, W. Han and I. V. Zatonvsky, *International Journal of Hydrogen Energy*,  
508 2021, **46**, 21462-21474.
- 509 71. B. K. Martini, L. S. Bezerra, S. Artemkina, V. Fedorov, P. K. Boruah, M. R. Das and G. Maia,  
510 *Chemical Engineering Journal Advances*, 2022, **9**, 100206.
- 511 72. A. Hanan, M. Ahmed, M. N. Lakhan, A. H. Shar, D. Cao, A. Asif, A. Ali and M. Gul, *Journal of  
512 the Indian Chemical Society*, 2022, **99**.
- 513 73. S. Parvin, D. K. Chaudhary, A. Ghosh and S. Bhattacharyya, *ACS Applied Materials &  
514 Interfaces*, 2019, **11**, 30682-30693.
- 515 74. R.-Y. Fan, J.-Y. Xie, N. Yu, Y.-M. Chai and B. Dong, *International Journal of Hydrogen  
516 Energy*, 2022, **47**, 10547-10572.
- 517 75. T. Zhang, S.-A. Liao, L.-X. Dai, J.-W. Yu, W. Zhu and Y.-W. Zhang, *Science China Materials*,  
518 2018, **61**, 926-938.
- 519 76. J.-X. Guo, S.-Y. Wu, G.-J. Zhang, L. Yan, J.-G. Hu and X.-Y. Li, *Journal of Colloid and  
520 Interface Science*, 2022, **616**, 177-188.

521

522

523

524

## Supplementary Information

525

### **PdO@CoSe<sub>2</sub> Composites: An Efficient Electrocatalysts for Water Oxidation in Alkaline Media**

527

528 Abdul Hanan<sup>a</sup>, Muhammad Yameen Solangi<sup>b</sup>, Abdul Jaleel Iaghari<sup>b</sup>, Aqeel Ahmed Shah<sup>c</sup>, Umair  
529 Aftab<sup>\*,b</sup>, Zahoor Ahmed Ibupoto, Muhammad Ishaque Abro<sup>b</sup>, Muhammad Nazim Lakhani<sup>a</sup>, Irfan  
530 Ali<sup>d</sup>, Elmuez A. Dawi<sup>e</sup>, Abd Al Karim Haj Ismail<sup>e</sup>, Elfathi Mustafa<sup>f</sup>, Brigitte Vigolo<sup>h</sup>, Aneela  
531 Tahira<sup>i</sup>, Zafar Hussain Ibupoto<sup>\*,g</sup>

532 <sup>a</sup>Key Laboratory of Superlight Material and Surface Technology, Ministry of Education, College  
533 of Materials Science and Chemical Engineering, Harbin Engineering University, 150001,  
534 Harbin, PR China.

535 <sup>b</sup>Department of Metallurgy and Materials Engineering, Mehran University of Engineering and  
536 Technology, 76080, Jamshoro, Pakistan.

537 <sup>c</sup>NED University of Engineering and Technology, 75270, Karachi, Pakistan.

538 <sup>d</sup>Institute of Computational Chemistry, College of Chemistry, Beijing University of Chemical  
539 Technology, 100029, Beijing, PR China.

540 <sup>e</sup>Nonlinear Dynamics Research Centre (NDRC), Ajman University, P.O. Box 346, United Arab  
541 Emirates.

542 <sup>f</sup>Department of Science and Technology (ITN), Linköping University, Campus Norrköping,  
543 60174 Norrköping, Sweden

544 <sup>g</sup>Dr. M.A Kazi Institute of Chemistry University of Sindh, Jamshoro, 76080, Pakistan

545 <sup>h</sup>Université de Lorraine, CNRS, IJL, F-54000 Nancy, France

546 <sup>i</sup>Institute of Chemistry, Shah Abdul Latif University Khairpur Mirs, Sindh, Pakistan

547

548 **Corresponding author(s):** Zafar Hussain Ibupoto and Umair Aftab

549 **E-mail:** zaffar.ibhupoto@usindh.edu.pk, umair.aftab@faculty.muuet.edu.pk

550

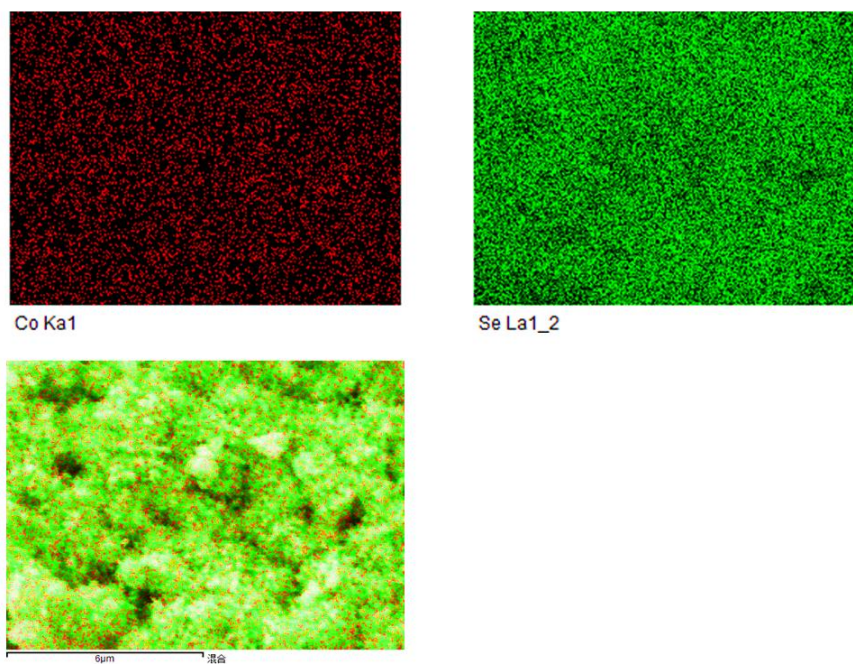


**Fig. S1** The elemental mapping of CoSe<sub>2</sub> pristine

551

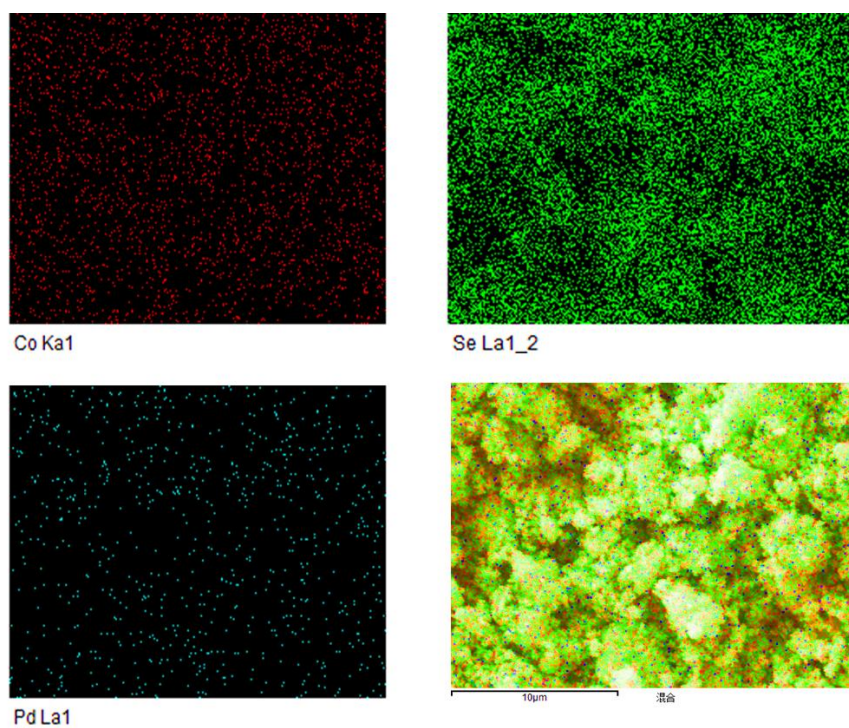


**Fig. S2** The elemental mapping of CSPd-2 nanostructure<sub>2</sub>

552

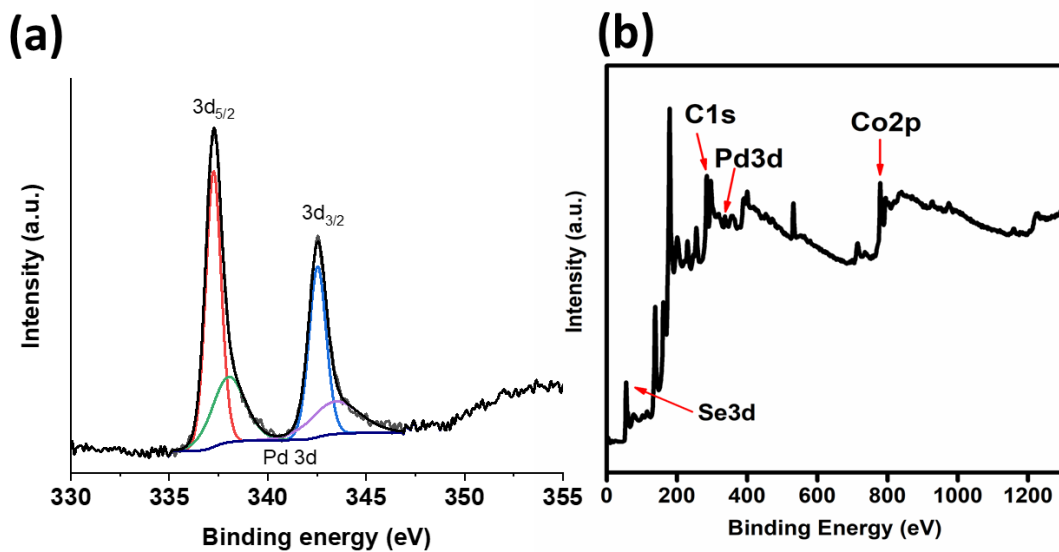


**Fig. S3** (a) Pd3d XPS spectra of CSPd-2 and (b) Main survey XPS analysis of CSPd-2 composite materials

553

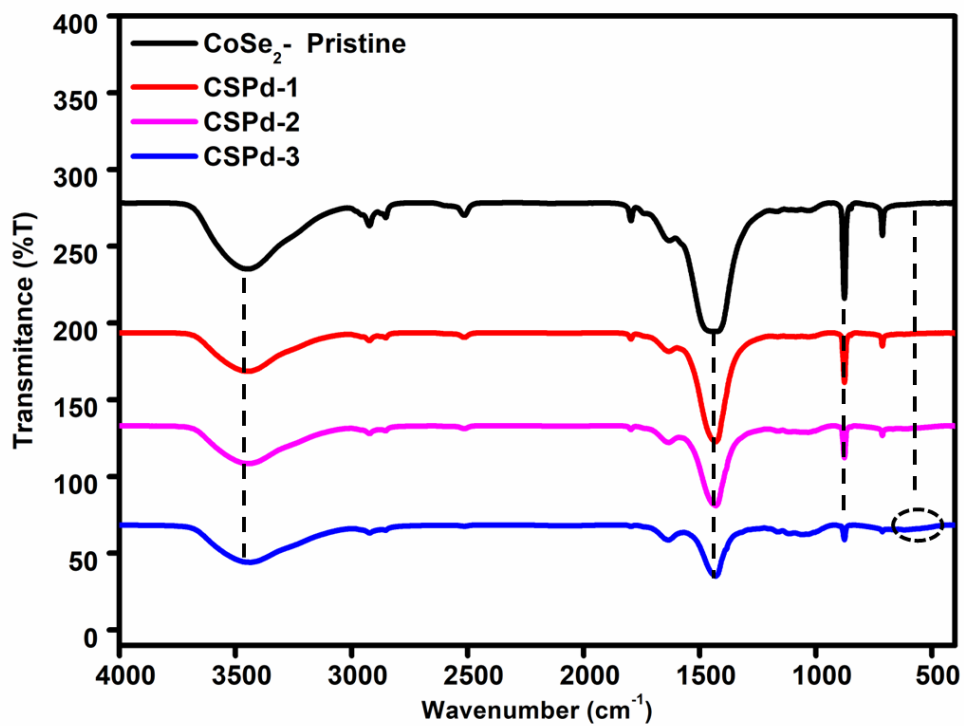


**Fig. S4** FTIR spectra of various nanostructures CoSe<sub>2</sub>, CSPd-1, CSPd-2 and CSPd-2

554

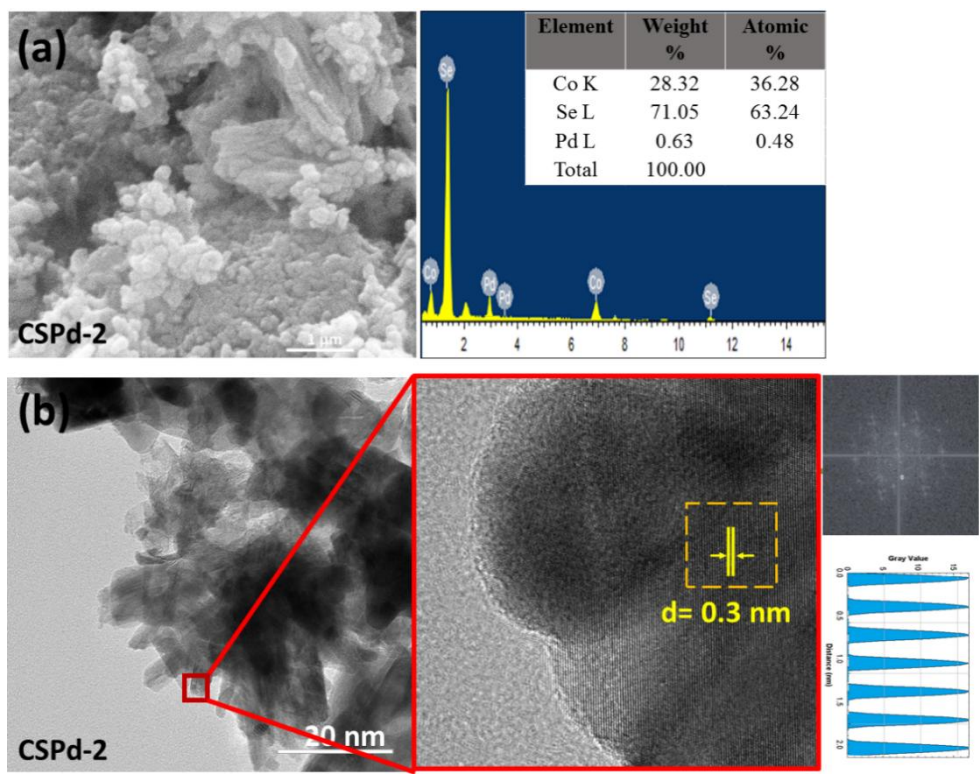


**Fig. S5** (a) SEM and EDS results after chronopotentiometry for sample CSPd-2 (b) HRTEM image with relevant FFT and lattice fringes calculation

555

556



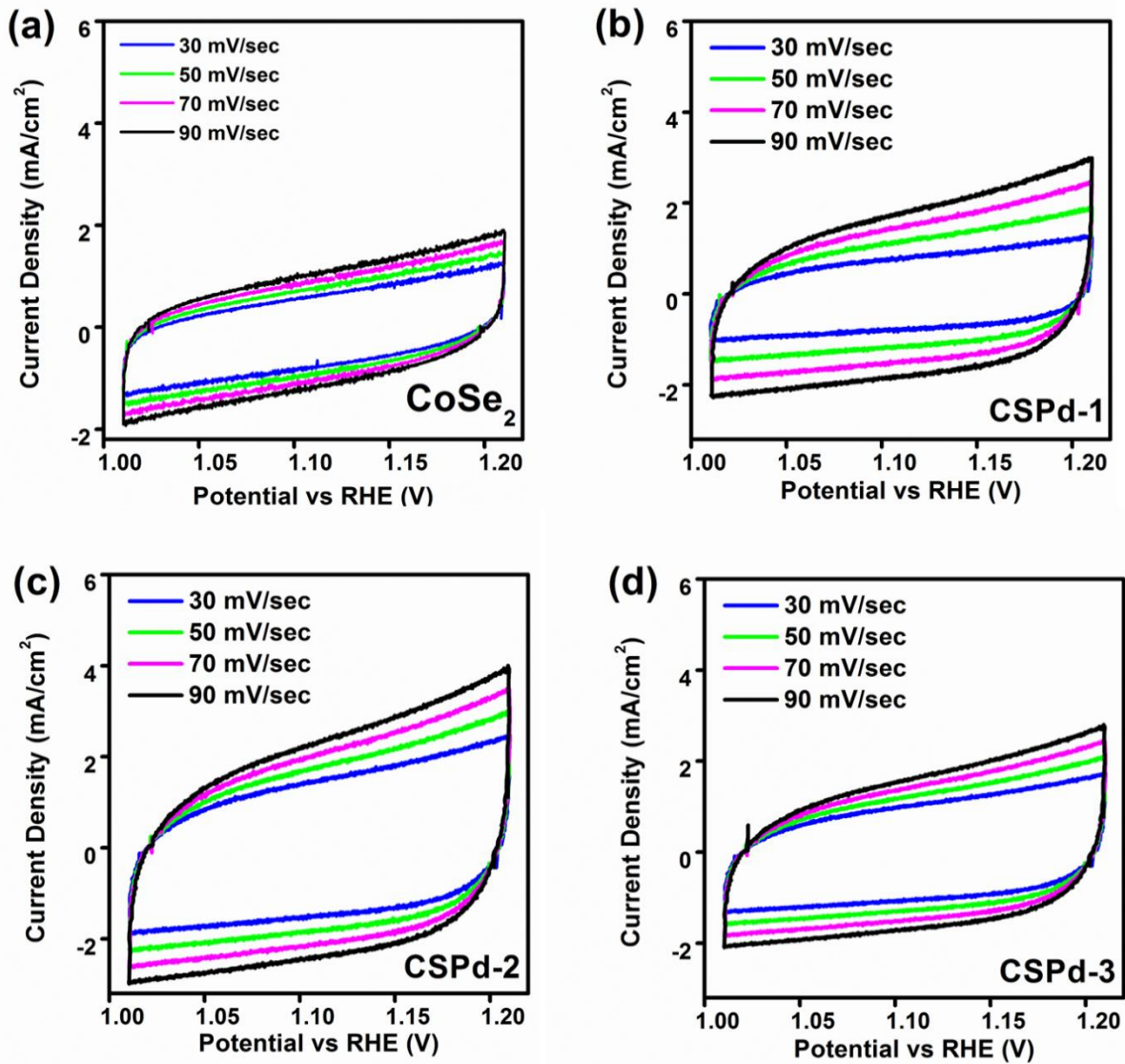


**Fig. S6** CV curves of various nanostructures to determine corresponding double layer capacitance values (a) CoSe<sub>2</sub>, (b) CSPd-1, (c) CSPd-2 and (d) CSPd-3

557

558

**Table S1.** Comparison with previously reported work toward OER

| Catalyst   | Electrolyte  | Overpotential | Tafel slope | Reference No.    |
|--|--------------|---------------|-------------|------------------|
|  | KOH          | mV            | mV/Dec      |                  |
| <b>CSPd-2</b>  | <b>1.0 M</b> | <b>260</b>    | <b>57</b>   | <b>This work</b> |
| CoSe <sub>2</sub> ultrathin nanosheets   | 1.0 M        | 320           | 44          | 1                |
| Ag-CoSe <sub>2</sub>   | 1.0 M        | 320           | 56          | 2                |
| CoSe and Co <sub>9</sub> Se <sub>8</sub>   | 1.0 M        | 280           | 40          | 3                |
| NiSe <sub>2</sub> /g-C <sub>3</sub> N <sub>4</sub>                                       | 1.0 M        | 290           | 143         | 4                |
| Ni <sub>3</sub> Se <sub>2</sub>  | 0.3 M        | 280           | 79.5        | 5                |
| Two-tiered NiSe  | 1.0 M        | 290           | 77          | 6                |
| Cu <sub>2</sub> Se   | 1.0 M        | 270           | 48          | 7                |
| Ni <sub>3</sub> Se <sub>2</sub>  | 1.0 M        | 290           | 80          | 8                |
| Cu-14-Co <sub>3</sub> Se <sub>4</sub>  | 0.1 M        | 280           | 110         | 9                |
| NiCo <sub>2</sub> Se <sub>4</sub>  | 1.0 M        | 295           | 53          | 10               |
| Co-Ni-Se/carbon/Ni foam  | 1.0 M        | 275           | 63          | 11               |
| (Co <sub>0.21</sub> Ni <sub>0.25</sub> Cu <sub>0.54</sub> ) <sub>3</sub> Se <sub>2</sub> | 1.0 M        | 272           | 53.3        | 12               |
| ZnNi <sub>0.5</sub> Co <sub>0.5</sub> Se <sub>2</sub> /Cu <sub>1.8</sub> Se@carbon cloth | 1.0 M        | 370           | 72          | 13               |

562 **References**

- 563 1. Y. Liu, H. Cheng, M. Lyu, S. Fan, Q. Liu, W. Zhang, Y. Zhi, C. Wang, C. Xiao, S. Wei, B. Ye  
564 and Y. Xie, *Journal of the American Chemical Society*, 2014, **136**, 15670-15675.
- 565 2. X. Zhao, H. Zhang, Y. Yan, J. Cao, X. Li, S. Zhou, Z. Peng and J. Zeng, *Angewandte Chemie*  
566 *(International ed. in English)*, 2017, **56**, 328-332.
- 567 3. H. Zhou, F. Yu, Y. Liu, J. Sun, Z. Zhu, R. He, J. Bao, W. A. Goddard, S. Chen and Z. Ren,  
568 *Energy & Environmental Science*, 2017, **10**, 1487-1492.
- 569 4. S. Wang, P. He, L. Jia, M. He, T. Zhang, F. Dong, M. Liu, H. Liu, Y. Zhang, C. Li, J. Gao and L.  
570 Bian, *Applied Catalysis B: Environmental*, 2019, **243**, 463-469.
- 571 5. A. T. Swesi, J. Masud and M. Nath, *Energy & Environmental Science*, 2016, **9**, 1771-1782.
- 572 6. H. Wu, X. Lu, G. Zheng and G. W. Ho, *Advanced Energy Materials*, 2018, **8**, 1702704.
- 573 7. J. Masud, W. P. R. Liyanage, X. Cao, A. Saxena and M. Nath, *ACS Applied Energy Materials*,  
574 2018, **1**, 4075-4083.
- 575 8. J. Zhang, Y. Wang, C. Zhang, H. Gao, L. Lv, L. Han and Z. Zhang, *ACS Sustainable Chemistry*  
576 *& Engineering*, 2018, **6**, 2231-2239.
- 577 9. J. Dai, D. Zhao, W. Sun, X. Zhu, L.-J. Ma, Z. Wu, C. Yang, Z. Cui, L. Li and S. Chen, *ACS*  
578 *Catalysis*, 2019, **9**, 10761-10772.
- 579 10. Z. Fang, L. Peng, H. Lv, Y. Zhu, C. Yan, S. Wang, P. Kalyani, X. Wu and G. Yu, *ACS nano*,  
580 2017, **11**, 9550-9557.
- 581 11. F. Ming, H. Liang, H. Shi, X. Xu, G. Mei and Z. Wang, *Journal of Materials Chemistry A*, 2016,  
582 **4**, 15148-15155.
- 583 12. X. Cao, E. Johnson and M. Nath, *Journal of Materials Chemistry A*, 2019, **7**, 9877-9889.
- 584 13. H. Hosseini and S. Shahrokhian, *Chemical Engineering Journal*, 2019, **375**, 122090.

585